OPEN ACCESS
Saudi Journal of Engineering and Technology
Abbreviated Key Title: Saudi J Eng Technol
ISSN 2415-6272 (Print) |ISSN 2415-6264 (Online)
Scholars Middle East Publishers, Dubai, United Arab Emirates
Journal homepage: https://saudijournals.com

Review Article

Power-Law Fluid Flow and Heat Transfer via Vertical, Parallel Porous Walls with Varying Thermal Conductivity and Viscosity, As Well As Nth Order Chemical Reaction

Hussaini Abdullahi[1*], Ahmad Rufai[1], Sadiq Shehu Yabo[1]

[1]Sokoto State University, Sokoto, Nigeria

DOI: 10.36348/sjet.2022.v07i11.003 | **Received:** 08.11.2022 | **Accepted:** 17.12.2022 | **Published:** 23.12.2022

***Corresponding author:** Hussaini Abdullahi
Sokoto State University, Sokoto, Nigeria

Abstract

This analysis examines a non-uniform heat source or sink, the flow of a power-law fluid induced by vertical parallel plates, and heat transfer using variable viscosity and thermal conductivity. Temperature likely exponentially changes viscosity and thermal conductivity. The implicit finite difference approach solves governing partial differential equations. Power-law index, Prandtl number, variable viscosity, and thermal conductivity are analysed. Skin friction, Nusselt number, and Sherwood number are graphically depicted to analyse channel fluid behaviour.

Keywords: Power-law fluid; variable viscosity; variable thermal conductivity; implicit finite difference method.

1. INTRODUCTION

Recent years have seen a rise in the importance of non-Newtonian fluid due to its many industrial uses. Numerous studies concentrate on the foundation fluid, a non-Newtonian fluid over a stretching sheet, with distributed nanoparticles. In the past ten years, non-Newtonian fluid mechanics has gained a great deal of attention, partly due to its numerous applications in the chemical and pharmaceutical industries. Non-Newtonian fluid mechanics is gaining more and more attention in the scientific community. Non-Newtonian fluids are easily identifiable in a wide range of processes, including those involving waste fluids, synthetic fibers, and polymer solutions as well as those involving the extraction of molten plastic. The range of fluids and industrial applications has been a key source of inspiration for non- Newtonian flow researchers. Newtonian fluids and non-Newtonian fluids have entirely distinct flow properties. Non- Newtonian power-law fluids have been used in a wide range of scientific and technical disciplines, including metallurgy, polymer extrusion, glass blowing, crystal formation, and others, to enhance the understanding of flow and heat-mass transfer. Numerous researches has comprehensively investigated fluid flow and heat transfer from channels in cross flow to Newtonian fluids at the theoretical, experimental, and computational levels. But according to Khan *et al.*, [1], these experiments are exceedingly uncommon for non-Newtonian fluids, especially for power law fluids. Acrivos *et al.*, [2] used an analytical-numerical approach to conduct the first theoretical research of forced convective heat transfer from an isothermal flat plate to power-law fluids. Later, Schowalter [3], Shah *et al.*, [4], Acrivos *et al.*, [5], and Lee and Ames [6] devised similarity transformations for the solution of 2-D boundary layer equations. Research by Memon *et al.*, [7] into non-Newtonian fluid flow and heat transfer with implications for the fluid's power law on the interacting surface led to the discovery of locations of separation for different values of the power-law index by analysing the boundary layer on a sphere using the Von Karman-Pohlhausen integral technique.

Due to its technical and commercial applications, research into the flow, heat, and mass transfer of spontaneous convection of non-Newtonian fluids in porous media has attracted a lot of attention. These objectives include the production and dispersion of fog, temperature and moisture distributions over agricultural fields and orchards, freezing- related crop damage, environmental contamination, etc. Convection of heat and mass transfer issues has been expanded by relevant researchers to include fluids with non-Newtonian rheology. In order to describe the behaviour of non- Newtonian fluids, numerous models have been

developed. The power law model rose to prominence among them. Despite being just an empirical relationship between stress and velocity gradients, this model has been effectively used in studies with non-Newtonian fluids. Nakayama [8] investigated free convection from a horizontal line heat source in a power-law fluid-saturated porous material. Sahu and Mathur [9] studied free convection in boundary layer flows of power law fluids past a vertical flat plate with suction/injection. They found that the suction/injection had a considerable impact on the temperature and velocity fields. Rami and Arun [10] investigated the free convection heat and mass transport of non-Newtonian power law fluids with yield stress from a vertical flat plate in a saturated porous environment. They came to the conclusion that the fluid rheology, along with the fluid's buoyancy ratio and Lewis number, has a significant impact on the velocity, temperature, and concentration profiles, as well as the local heat and mass transfer rates. Cheng [11] took into consideration the non-Newtonian power law fluid flow of natural convection heat and mass transfer with yield stress in porous medium from a vertical plate with varying wall heat and mass fluxes. He discovered that the local Nusselt and Sherwood numbers and fluid velocity tend to drop in power law fluids when there is a threshold pressure differential. The Nusselt and Sherwood values rose together with the local power law exponent. The focus of an analysis by Kairi and Murthy [12] was a vertical flat plate embedded in a thermally stratified non-Newtonian fluid-saturated non-Darcy porous media.

Flows that are buoyancy-driven and caused by both temperature and concentration gradients are known as double-diffusive convection. Double-diffusive natural convection is used in numerous engineering processes, including drying processes, contaminant transport in saturated soils, evaporative cooling of high temperature systems and underground disposal of nuclear wastes, contaminant spread, and crystal formation from liquid phase. These usages have motivated researchers to look into this phenomenon. A numerical analysis of double-diffusive convection in a rectangular cavity with coupled horizontal temperature and concentration gradients was done by Hyun and Lee [13]. In order to create an opposing gradient flow arrangement, they imposed boundary limitations at the vertical side walls in a way that the thermal and solutal buoyancy effects are counteracting. Goyeau *et al.,* [14] performed a computer examination of double-diffusive natural convection in a porous cavity using the Darcy Brinkman model. They discovered that the Darcy number considerably affects heat transfer, which is more complex than thermal convection and deviates greatly from the fluid behaviour that was initially predicted. Double diffusive convection in a vertical enclosure has been studied analytically and quantitatively by Mamou *et al.,* [15]. The two extreme instances of heat- and mass-driven flows were scale-analyzed in his analytical investigation, and he later gave an analytical solution based on the parallel flow approximation for tall enclosures. In a porous media that was fluid-saturated and had consistent wall temperatures and concentrations, Cheng [16] investigated the double diffusive natural convection close to an inclined wavy surface. The complex wavy surface was turned into a smooth surface by a coordinate transformation, and the boundary layer equations were then solved by the cubic spine collocation technique.

The works mentioned above focus on the cooling liquid's constant physical properties, whereas real-world scenarios necessitate a variety of physical qualities. One such attribute that is thought to change linearly with temperature is thermal conductivity Kays and Grawford [17]. Chiam [18, 19] thought about the potential effects of thermal conductivity differences on heat transmission. In the presence of thermal radiation and the buoyancy force, Abel *et al.,* [20] investigated the effects of changing thermal conductivity on the MHD boundary layer viscoelastic fluid flow. Natural convection flow with variable viscosity and thermal conductivity has been thoroughly and in-depth examined by Animasaun [21], Kiran *et al.,* [22], Babu *et al.,* [23], Choudhury and Hazarika [24], among others. Using a stretching surface encased in a saturated porous media, Swain *et al.,* [25] have described continuous two-dimensional stagnation point flow of an incompressible conducting viscous fluid with changing characteristics.

According to a review of the literature, no studies have been done on the problem of temperature-dependent variable viscosity and thermal conductivity with Soret and Dufour effects, double diffusive natural convection heat, and mass transfer from a vertical plate in Darcy porous media saturated in power-law fluid. In this work, the effect of Soret and Dufour on double-diffusive natural convection in a power-law fluid immersed in a porous Darcy medium with varying surface temperature and concentration is the main topic of investigation. Thermal conductivity and fluid viscosity are thought to be exponential functions of temperature. The governing boundary layer equations are first expressed in their dimensionless form for implicit finite difference solution of the resulting system of equations.

2. Formulations of Problem

Figure 1 shows natural convection heat and mass movement down a vertical plate in a Darcy porous non- Newtonian fluid. Choose a coordinate system with the x-axis vertical and the y-axis horizontal. At time $t' = 0$, the plate's surface temperature T_w and concentration C_w are variable. T_h and C_h are the medium's temperature and concentration. Assume the fluid and porous materials have constant physical

parameters other than density. Unsteady, two-dimensional laminar flow. Isotropic, uniform porous media. Fluid and porous medium are thermodynamically balanced. Soret and Dufour impacts are considered. Under these conditions, the fluid flow governing equations are:

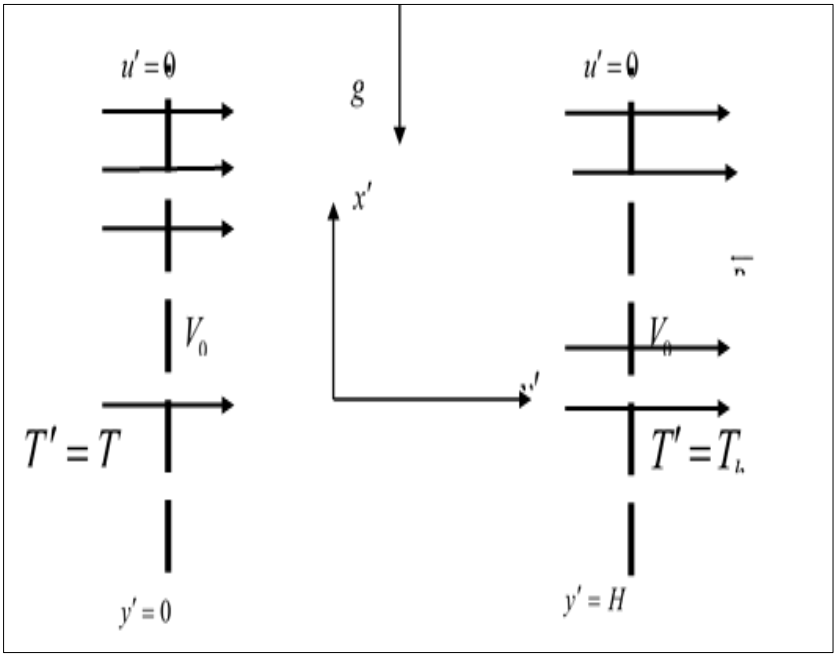

Fig. 1: Schematic diagram of Problem

Continuity equation

$$\frac{\partial v'}{\partial y'} = 0 \tag{1}$$

Momentum equation

$$\frac{\partial u'}{\partial t'} + v'\frac{\partial u'}{\partial y'} = \frac{1}{\rho}\frac{\partial}{\partial y'}\left[\mu(T)\left|\frac{\partial u'}{\partial y'}\right|^{n-1}\frac{\partial u'}{\partial y'}\right] + g\beta\left(T'-T_h'\right) + g\beta^*\left(C'-C_h'\right) - \frac{\sigma\beta_0^2}{\rho}u' - \frac{\upsilon}{k'}u' - F^*u'^2 \tag{2}$$

Heat transfer equation

$$\frac{\partial T'}{\partial t'} + v'\frac{\partial T'}{\partial y'} = \frac{1}{\rho c_p}\frac{\partial}{\partial y'}\left\{k(T)\frac{\partial T'}{\partial y'}\right\} + \frac{QC_0^{\bullet}A}{\rho c_p}\exp\left(\frac{-E}{RT}\right) + \frac{\mu}{c_p}\left(\frac{\partial u'}{\partial y'}\right)^2 + \ldots$$

$$\frac{D_m K_T}{C_s C_p}\frac{\partial^2 C'}{\partial y'^2} + \frac{Q_0}{\rho c_p}\left(T'-T_h'\right) + b^*u'^2 \tag{3}$$

Mass transfer equation

$$\frac{\partial C'}{\partial t'} + v'\frac{\partial C'}{\partial y'} = D\frac{\partial^2 C'}{\partial y'^2} - R\left(C'-C_h'\right)^q + \frac{D_m K_T}{T_M}\frac{\partial^2 T'}{\partial y'^2} \tag{4}$$

The initial and boundary conditions are :

$$t' \le 0 : u' = 0, T' = T_0, C' = C_0 \text{ for } 0 \le y' \le H$$

$$t' > 0 : \begin{cases} u' = 0, T' = T_w, C' = C_w \text{ at } y' = 0 \\ u' = 0, T' = T_0, C' = C_0 \text{ at } y' = H \end{cases} \tag{5}$$

Where u, v are the velocity components in x, y directions respectively, t' , the time, g, the acceleration due to gravity, β , the volumetric coefficient of thermal expansion, β^* , the volumetric coefficient of expansion with concentration, T' , the temperature of the fluid in the boundary layer, C', the species concentration in the boundary layer, υ , the kinematic viscosity, σ , the electrical conductivity, B_0 , the magnetic induction, ρ , the density of the fluid, c_p ,the specific heat at constant pressure, q_r ,the radiation heat flux, Q_0 , the heat generation/absorption and D , the species diffusion coefficient, F^* , the Forchheimer parameter, b^* , the Hall current parameter.

In terms of dimensionless temperature T the fluid viscosity and thermal conductivity is written as:

$$\mu = \mu_0 \exp(-\lambda T) \tag{6}$$

$$k = k_0 \exp(-\gamma T) \tag{7}$$

Where λ and γ are the viscosity parameter and thermal conductivity parameter respectively and μ_0, k_0 are the dynamic viscosity and thermal conductivity respectively at temperature T_w'.

Inserting non-dimensional dependent and independent variables according to:

$$x' = \frac{x}{H}, y' = \frac{yGr^{1/4}}{H}, t' = \frac{tH^2Gr^{-1/2}}{\nu}, u' = \frac{uGr^{-1/2}}{\nu}, Gr = \frac{g\beta H^3(T_w' - T_h)}{\nu^2}, \phi = \frac{Q_0 H^2}{\rho c_p \nu Gr^{1/2}},$$

$$T = \frac{T' - T_h'}{T_w' - T_h'}, C = \frac{C' - C_h'}{C_w' - C_h'}, \Pr = \frac{\nu}{\alpha}, F = \frac{k_e k}{4\sigma_s T_h'^3}, Sc = \frac{\nu}{D}, Ec = \frac{u_0^2}{c_p(T_w' - T_h')}, N = \frac{\beta^*(C_w' - C_h')}{\beta(T_w' - T_h')}$$

$$M = \frac{\sigma B_0^2}{u_0^2}, T_1 = \frac{E(T' - T_h)}{RT_h^2}, \delta = \frac{QC_0^* AEH^2}{RT_h^2} e^{\left(\frac{-E}{RT_h}\right)}, \varepsilon = \frac{RT_h}{E} \quad Fr = \frac{F^*\nu}{T_w' - T_h'}, b = \frac{b^*\nu}{u_0} \tag{8}$$

Where H is the reference length, υ is the kinematic viscosity, *Gr* is the Grashof number, Pr is Prandtl number and Sc is Schmidt number.

Substituting equation (8) in equations (2), (3), (4) and (5) give the following:

$$\frac{\partial u}{\partial t} + \eta \frac{\partial u}{\partial y} = \exp(-\lambda T) \frac{\partial^2 u}{\partial y^2} \left| \frac{\partial u'}{\partial y'} \right|^{n-1} - \lambda \exp(-\lambda T) \frac{\partial u}{\partial y} \frac{\partial T}{\partial y} \left| \frac{\partial u'}{\partial y'} \right|^{n-1} + T + NC - \left(M + \frac{1}{Da\,\mathrm{Re}} \right) u + Fru^2 \tag{9}$$

$$\Pr\left[\frac{\partial T}{\partial t} + \eta \frac{\partial T}{\partial y} \right] = \exp(-\gamma T) \frac{\partial^2 T}{\partial y^2} - \gamma \exp(-\gamma T) \left(\frac{\partial T}{\partial y} \right)^2 + \Pr Ec \left(\frac{\partial u}{\partial y} \right)^2 + \ldots$$

$$\delta \exp\left(\frac{T_1}{1 + \varepsilon T} \right) + Du \frac{\partial^2 C}{\partial y^2} + \Pr bu^2 + \Pr \phi T \tag{10}$$

$$Sc\left[\frac{\partial C}{\partial t} + \eta \frac{\partial C}{\partial y} \right] = \frac{\partial^2 C}{\partial y^2} + ScSr \frac{\partial^2 T}{\partial y^2} - ScKcC^{n'} \tag{11}$$

The corresponding initial and boundary conditions are

$$t>0:\ \begin{cases} u=0, & T=1, C=1 \quad at\ \ y=0 \\ u=0, & T=0, C=0 \quad at\ \ y=1 \end{cases} \tag{12}$$

Where η is the suction/injection parameter, γ is the thermal conductivity parameter, M is the magnetic parameter, s $\Pr$ is the Prandtl number, Ec is the Ekert number, N is the buoyancy parameter, ϕ is the dimensionless heat generation/absorption coefficient, λ is the variable viscosity parameter and Sc is the Schmidt number, Fr is the inertia number, b is the Hall current. Recognizing the velocity, temperature and concentration field, it is standard to study the physical quantities of fundamental interest of the skin-friction, the rate of heat transfer and Sherwood number in unsteady state conditions.

The dimensionless skin-friction, Nusselt number and Sherwood number can be expressed as:

$$C_f = \exp(-\lambda T)\left[\frac{\partial u}{\partial y}\right]_{y=0,1} \tag{13}$$

$$Nu = -\exp(-\gamma T)\left[\frac{\partial T}{\partial y}\right]_{y=0,1} \tag{14}$$

$$S_h = \left[\frac{\partial C}{\partial y}\right]_{y=0,1} \tag{15}$$

3. Numerical Procedures

The Equations (9)-(11) are solved by implicit finite difference method. As discretization in space and time a consistent mesh of step Δy along the y direction and time Δt are used so that the grid points are $(y_j, t_k) = (j\Delta y, j\Delta y)$, for $j = 1, 2, \ldots M$ and $k = 0, 1, 2, \ldots K$. The discretized form of -Equation (9), (10), (11) and (12) are obtained respectively as,

$$\frac{u_i^{j+1}-u_i^j}{\Delta t}+\eta\frac{(u_{i+1}^j-u_i^j)}{\Delta y}=\exp(-\lambda T_i^j)\left[\frac{u_{i+1}^{j+1}-2u_i^{j+1}+u_{i+1}^{j+1}}{\Delta y^2}\right]\left|\frac{u_{i+1}^j-u_i^j}{\Delta y}\right|^{n-1}-\lambda\exp(-\lambda T_i^j)\left[\frac{u_{i+1}^j-u_{i-1}^j}{2\Delta y}\right]\left[\frac{T_{i+1}^j-T_{i-1}^j}{2\Delta y}\right]\left|\frac{u_{i+1}^j-u_i^j}{\Delta y}\right|^{n-1}+\ldots$$

$$T_i^{j+1}+NC_i^{j+1}-\left(M+\frac{1}{Da\,\mathrm{Re}}\right)u_i^{j+1}+F(ru_i^l)^2 \tag{16}$$

$$\frac{\Pr(T_i^{j+1}-T_i^j)}{\Delta t}+\frac{\eta\Pr(T_{i+1}^j-T_i^j)}{\Delta y}=\frac{1}{\Pr\Delta y^2}\exp\left(-\gamma T_i^j\right)\left[T_{i-1}^{j+1}-2T_i^j+T_{i+1}^j\right]-\ldots$$

$$\frac{\gamma}{\Pr}\exp(-\gamma T_i^j)\left(\frac{T_{i+1}^j-T_{i-1}^j}{2\Delta Y}\right)^2+Ec\left(\frac{u_{i+1}^j-u_{i-1}^j}{2\Delta Y}\right)^2+\phi T_i^j+\delta e^{\left(\frac{T_i^j}{1+\varepsilon T_i^j}\right)}+\frac{Du}{\Delta Y^2}(C_{i-1}^j-2C_i^j+\ldots$$

$$C_{i+1}^j)+b\left(u_i^j\right)^2 \tag{17}$$

$$Sc\left(\frac{C_i^{j+1}-C_i^j}{\Delta t}\right)+\eta Sc\left(\frac{C_{i+1}^j-C_i^j}{\Delta y}\right)=\frac{1}{\Delta y^2}\left(C_{i-1}^j-2C_i^j+C_{i+1}^j\right)-ScKr(C_i^j)^{n'}+\ldots$$

$$\frac{ScSr}{\Delta y^2}(T_{i-1}^j-2T_i^j+T_{i+1}^j) \tag{18}$$

The above discretized Equations (13)-(15) are solved iteratively using the following algorithm.

Step I

Initialize $u_{i,j}^{(0)}, T_{i,j}^{(0)}, C_{i,j}^{(0)} \forall (i, j).$

Step II

For k= 0,1,2, 3…, k, max

For i= 1, 2…, N

For j= 1, 2…, M

$$C_i^{j+1} = \frac{1}{Sc} C_i^j - \eta r_3 (C_{i+1}^j - C_i^j) + \frac{r_1}{Sc}\left(C_{i-1}^j - 2C_i^j + C_{i+1}^j\right) - \Delta t Kc \left(C_i^j\right)^{n'} + r_1 Sr (T_{i-1}^j - 2T_i^j + T_{i+1}^j)$$

$$+\left(r_2 - \eta Scr_4\right) C_{i+1}^j + r_7 \left(T_{i-1}^j - 2T_i^j + T_{i+1}^j\right)$$

Step III

$$T_i^{j+1} = (1+\Delta t\phi) T_i^j - \eta r_3 (T_{i+1}^j - T_i^j) + \frac{r_1}{\Pr} \exp(-\gamma T_i^j)\left[T_{i+1}^j - 2T_i^j + T_{i+1}^j\right] - \frac{r_2 \gamma}{\Pr} \exp(-\gamma T_i^j)\left[T_{i+1}^j - T_{i-1}^j\right]^2 + \ldots$$

$$r_2 Ec\left[u_{i+1}^j - u_{i-1}^j\right]^2 - \Delta t b (u_i^j)^2 + \Delta t \delta \exp\left[\frac{T_i^j}{1+\varepsilon T_i^j}\right]$$

Step IV

$$u_i^{j+1} = \frac{u_i^j}{1 + M\Delta t + \Delta t (Da \operatorname{Re})^{-1}} + \frac{r_3}{1 + M\Delta t + \Delta t (Da \operatorname{Re})^{-1}} (u_{i+1}^j - u_i^j) + \ldots$$

$$\frac{r_1}{1 + M\Delta t + \Delta t (Da \operatorname{Re})^{-1}} \exp(-\lambda T_i^j)(u_{i+1}^j - 2u_i^j + u_{i+1}^j)\left|\frac{u_{i+1}^j - u_i^j}{\Delta y}\right|^{n-1} - \ldots$$

$$\frac{r_2 \lambda}{1 + M\Delta t + \Delta t (Da \operatorname{Re})^{-1}} \exp(-\lambda T_i^j)(u_{i-1}^j - 2u_i^j + u_{i+1}^j)(u_{i+1}^j - u_{i-1}^j)(u_{i+1}^j - u_{i-1}^j)\left|\frac{u_{i+1}^j - u_i^j}{\Delta y}\right|^{n-1} + \ldots$$

$$\frac{\Delta t}{1 + M\Delta t + \Delta t (Da \operatorname{Re})^{-1}} T_i^{j+1} + \frac{\Delta t}{1 + M\Delta t + \Delta t (Da \operatorname{Re})^{-1}} NC_i^{j+1} - \frac{\Delta t}{1 + M\Delta t + \Delta t (Da \operatorname{Re})^{-1}} Fr (u_i^j)^2$$

The steps (II)-(IV) are repeated until the relative errors of two consecutive values of $u_{i,j}^k, T_{i,j}^k, C_{i,j}^k$ are less than the tolerance.

Where $r_1 = \frac{\Delta t}{\Delta y^2}; \quad r_2 = \frac{\Delta t}{4\Delta y^2}; \quad r_3 = \frac{\Delta t}{\Delta y}; \quad r_4 = \frac{\Delta t}{\Delta y};$

4 RESULTS AND DISCUSSION

MHD boundary layer flow and heat transfer in an electrically conducting power-law fluid in a vertical infinite plate with varying viscosity and thermal conductivity is enquired in the presence of non-uniform heat source/sink. The flow is controlled by some basic parametric quantities, which are: buoyancy ratio (N), heat generating/absorbing (ϕ), variable viscosity parameter (λ), variable thermal conductivity (γ), Forchheimer parameter (Fr), power-law index (n) and Frank-Kamenetskii parameter. All round the value of $\Pr$ is taken to be $\Pr = 0.71$ for air and $\Pr = 7.0$ for water as working fluids. The solution for concentration, energy and momentum equations in the fluid have been solved for cautiously chosen values of the controlling parameters among the regime and the outcomes are depicted Figures 2-14.

Fig. 2 projects the influence of magnetic field (M) with suction and injection on the velocity profile. From this graph it is evident that the velocity decreases with increasing values of magnetic parameter (M). This is anticipated as the applied magnetic field induces a retarding force (Lorentz force) against the motion of the fluid enhancing the drag. Figure 3(a) and (b) map out the variation of the velocity profile for varied values

of buoyancy parameter (N) under two working fluids air $(\mathrm{Pr}=0.71)$ and electrolyze $(\mathrm{Pr}=1.0)$ severally. The plots exhibit marked increase in velocity. The effect of variable viscosity parameter (λ) is graphed in Figures 4(a) and 4(b) under the influence of suction and injection. As variable viscosity parameter (λ) grows the velocity increases in both shear thinning and shear thickening fluid. The outcomes of Darcy number (Da) is examined in plots 5(a) and 5(b) with varied values of Darcy number (Da). The Figures highlight that as Darcy number (Da) growths which entail a rise in permeability the velocity enhances.

The consequence of Prandtl number (Pr) on the temperature profile with suction $(\eta>0)$ and injection $(\eta<0)$ are projected in Figure 5(a) and 5(b) respectively. It is remarked that the temperature profile drop-offs with the varying values of Prandtl number (Pr) with both suction and injection. This is preferable to the reason that with the increasing values of the Prandtl number (Pr) the viscosity enhances and as a result temperature decreases. Figure 6(a) and 6(b) highlights temperature profile under different activation energy parameter (ε) in two different working fluid air $(\mathrm{Pr}=0.71)$ and water $(\mathrm{Pr}=7.0)$. It posited for different value of activation energy parameter (ε) the temperature is reduced in the boundary layer. The effect on the temperature curve is found in Figure 7(a) and 7(b), that is the temperature increases with increase of varying thermal conductivity parameter (γ) for power law index $(n=0.8)$ and the trend reverses for power law index $(n=1.6)$ with suction $(\eta>0)$ and injection $(\eta<0)$. Figures 8(a) and 8(b) depict the impact of heat source/sink parameter (ϕ) on temperature profile. It is noticed that the temperature profile gains with the increase of heat source/sink parameter (ϕ) in air $(\mathrm{Pr}=0.71)$ and water $(\mathrm{Pr}=7.0)$. Figures 9(a) and 9(b) project the influence of Frank-Kamenetskii parameter (δ) on the temperature profile with suction and injection. From this plot it is evident that the temperature heightens with increasing value of Frank-Kamenetskii parameter (δ). The results of Dufour number (Du) on the temperature profile are presented in Figures 10(a) and 10(b) in two working fluids, air $(\mathrm{Pr}=0.71)$ and water $(\mathrm{Pr}=7.0)$. It is emphasized that temperature growths with the varying Dufour number (Du).

The Schmidt number (Sc) examines the combined effect of momentum and mass diffusion. In figures 11(a) and 11(b), the effect of the Schmidt number (Sc) over the species concentration in the channel has been displayed for its various values. A comparison of curves in the Figure predicts a decrease in the concentration with an increase in the Schmidt number (Sc). Theoretically, the increase in Schmidt number (Sc) entails a decrease of the molecular diffusivity (D) that results in a decrease of the concentration boundary layer. Therefore, the concentration of the species is higher for small values of Schmidt number (Sc) and lower for larger values of Schmidt number (Sc). Figures 12(a) and 12(b) highlights the effects of Soret number (Sr) on the concentration profile under the influence of suction $(\eta>0)$ and injection $(\eta<0)$ in two working fluids, air $(\mathrm{Pr}=0.71)$ and water $(\mathrm{Pr}=7.0)$ with varying values of Soret number (Sr). It is observed in plot 12(a) that the concentration profile diminishes with increasing values of Soret number (Sr) with suction while it increases with injection as shown in Figure 12(b). The contribution of chemical reaction parameter (Kc) is pictured in Figures 13(a) and 13(b). It is examined from the plots that, growth in the chemical reaction parameter (Kc) contributes to the increase in the concentration of the fluid media. The results of chemical reaction parameter order (q) on the concentration profile are plotted in Figures 14(a) and 14(b). It is remarked that the concentration profile increases with the varying values of chemical reaction parameter order (q).

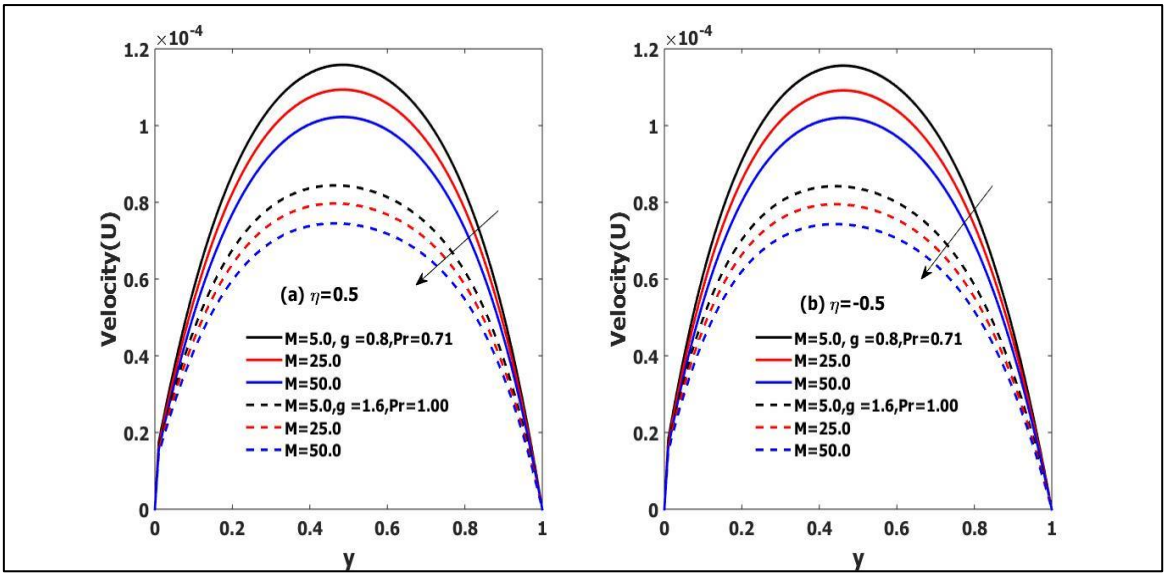

Figure 2: Interpretation of Magnetic parameter (M) on velocity profile

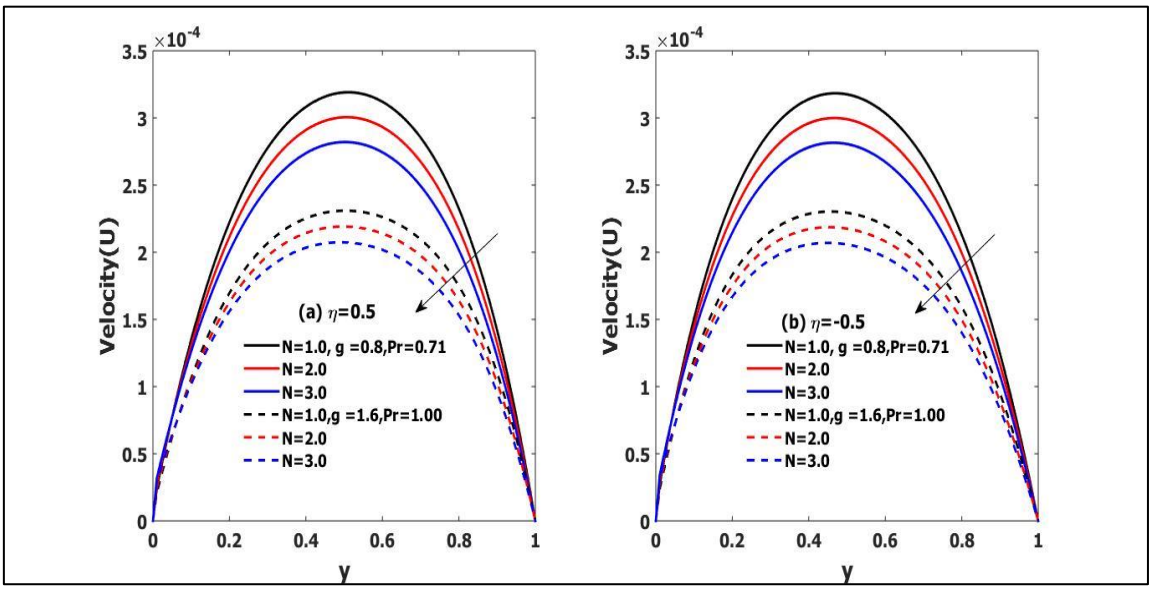

Figure 3: Interpretation of sustention parameter (N) on velocity profile

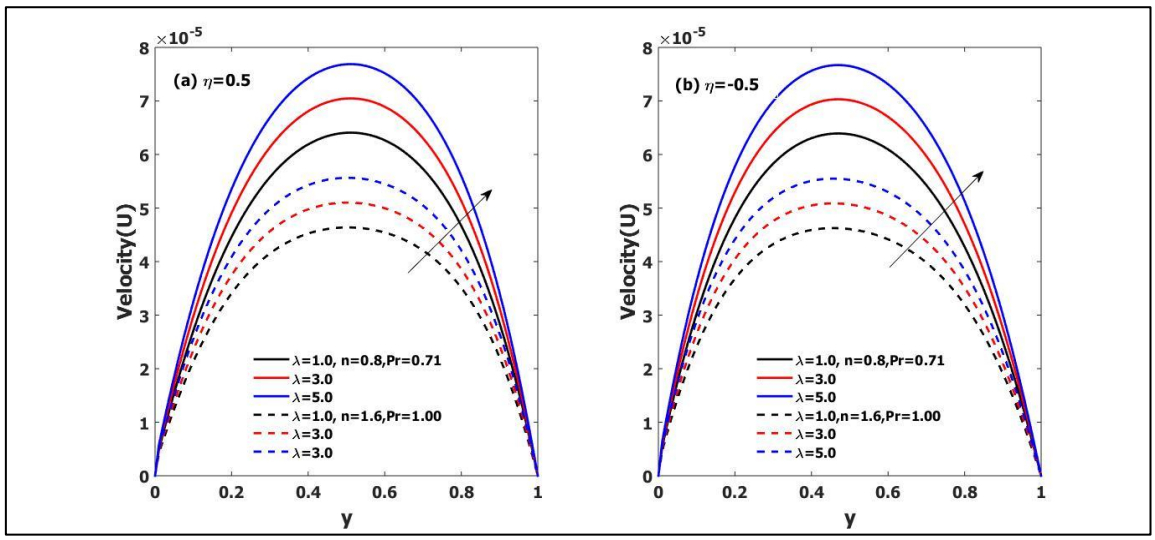

Figure 4: Interpretation of variable viscosity parameter on velocity profile

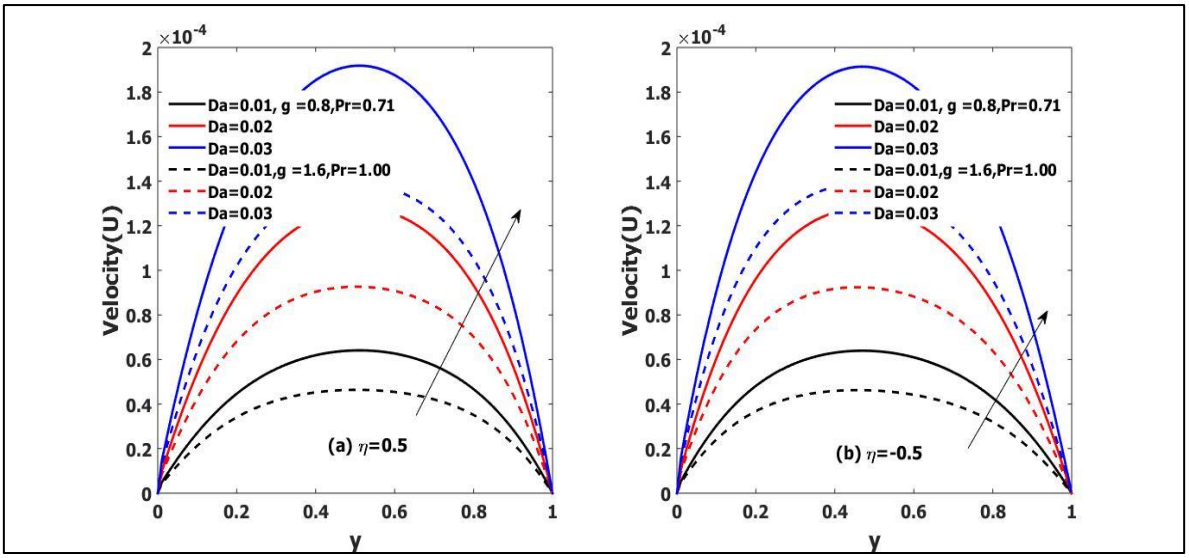

Figure 5: Interpretation of Darcy number (Da) on velocity profile

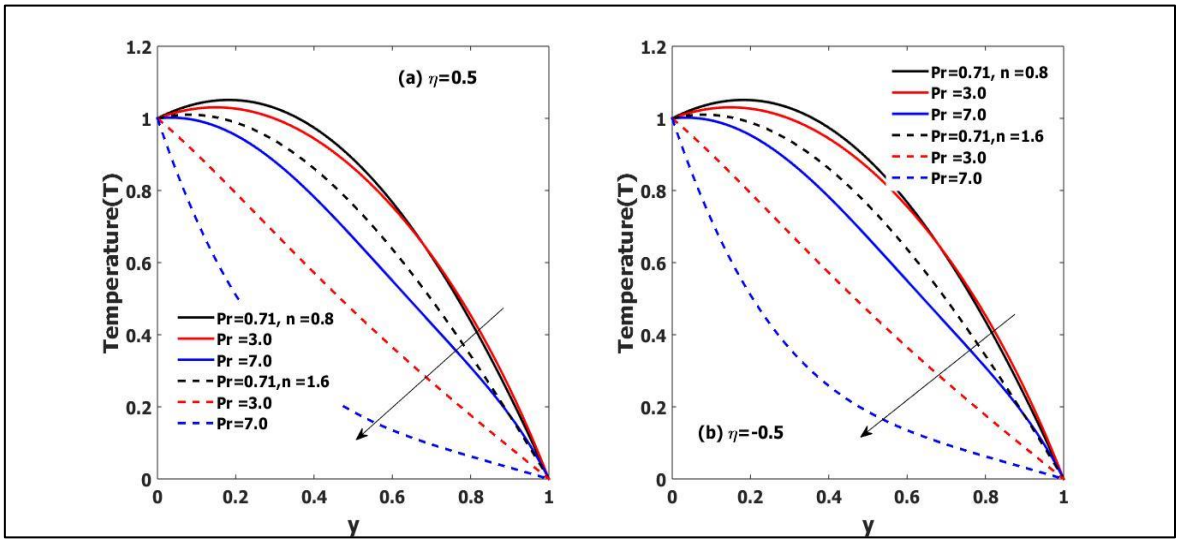

Figure 6: Interpretation of Prandtl number (Pr) on temperature profile

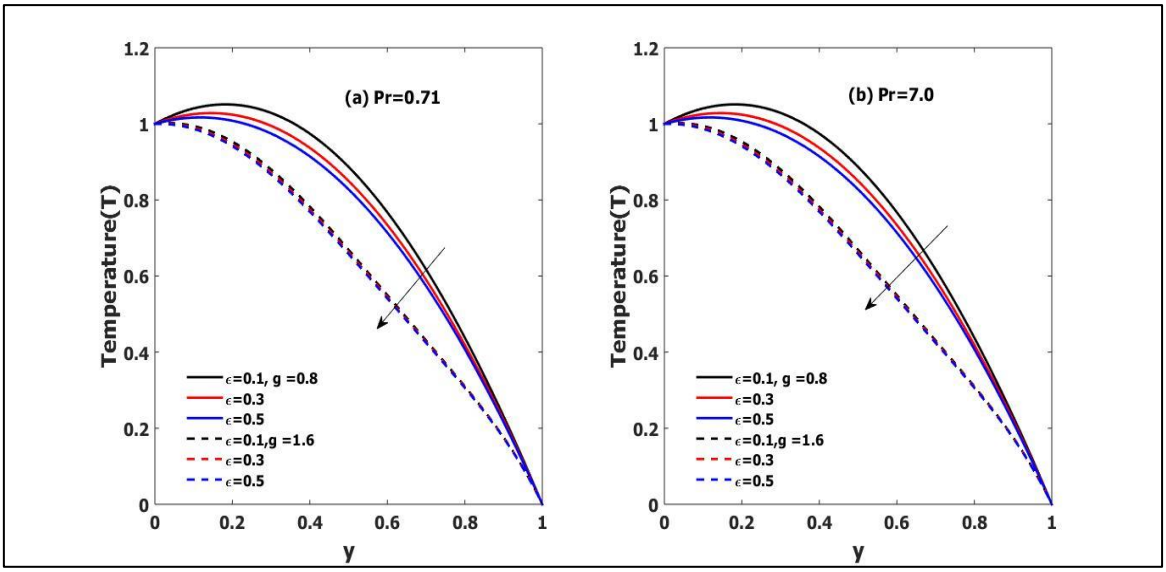

Figure 7: Interpretation of activation energy parameter (ε) on temperature profile

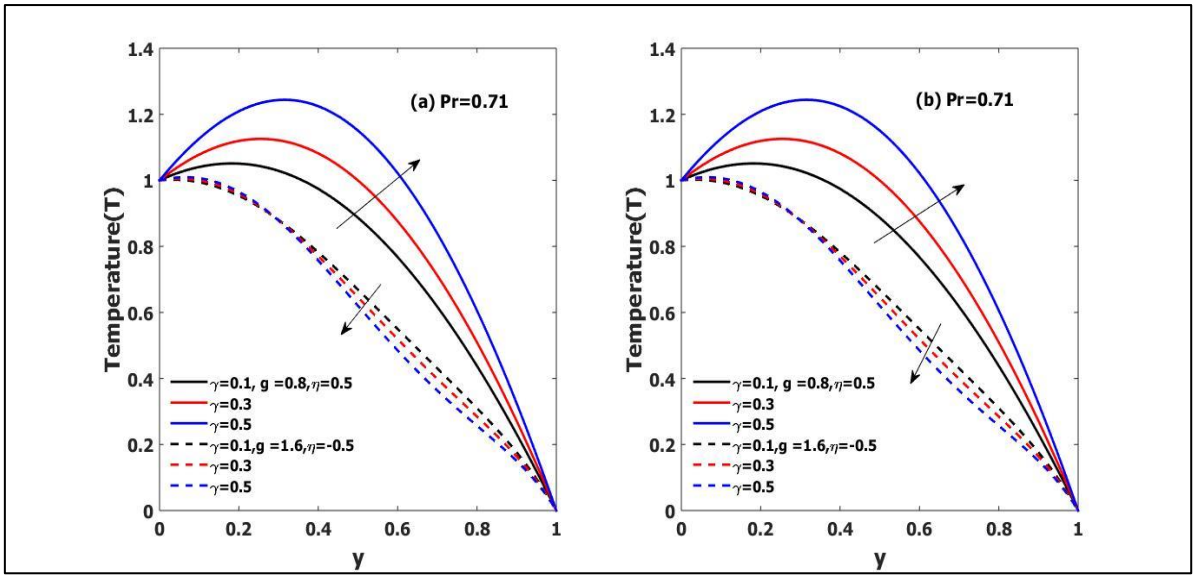

Figure 8: Interpretation of variable thermal conductivity parameter (γ) on temperature profile

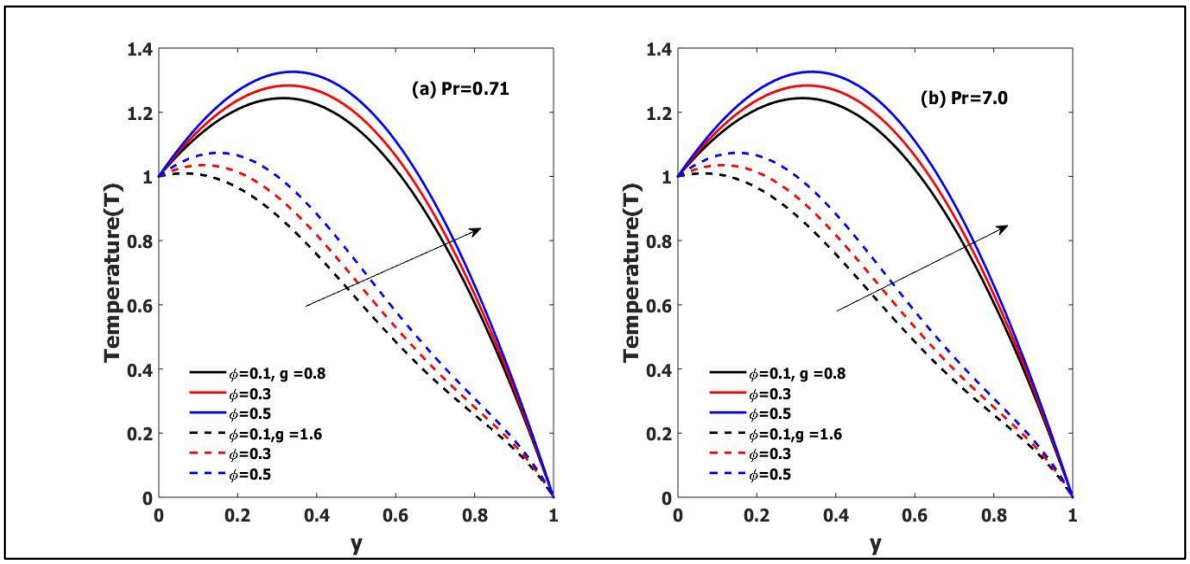

Figure 9: Interpretation of heat generation/absorption parameter (ϕ) on temperature profil

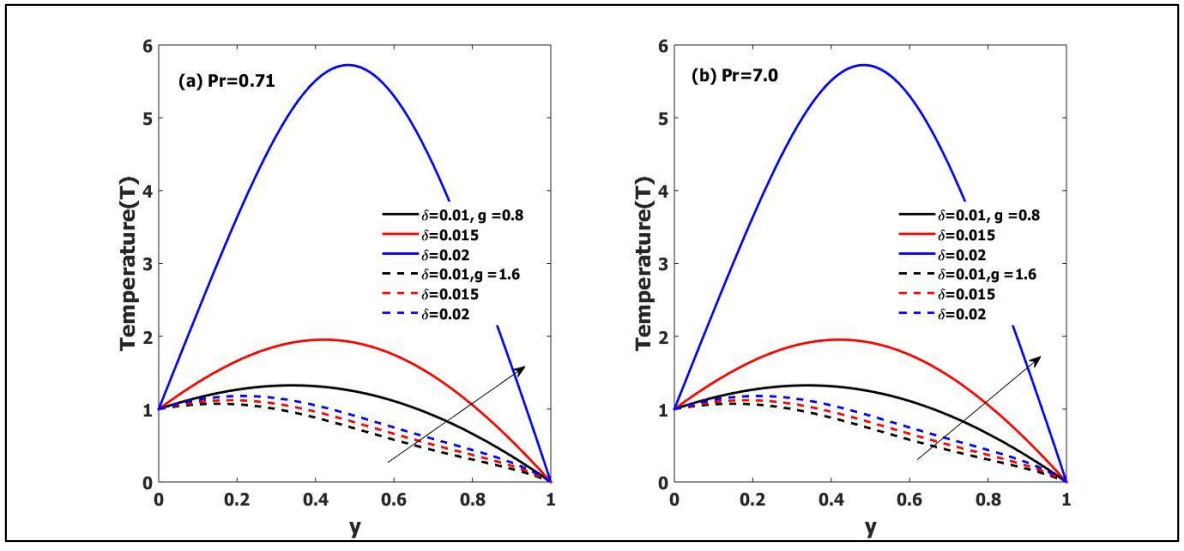

Figure 10: Interpretation of Frank-Kamenetskii parameter (δ) on temperature profile

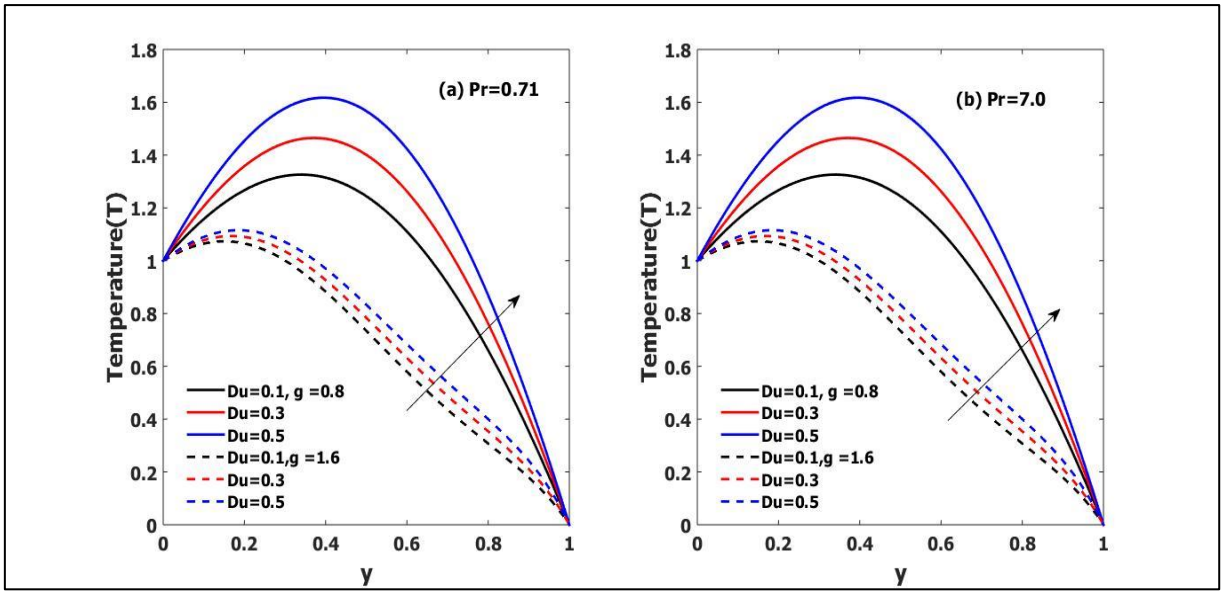

Figure 11: Interpretation of Dufour parameter (Du) on temperature profile

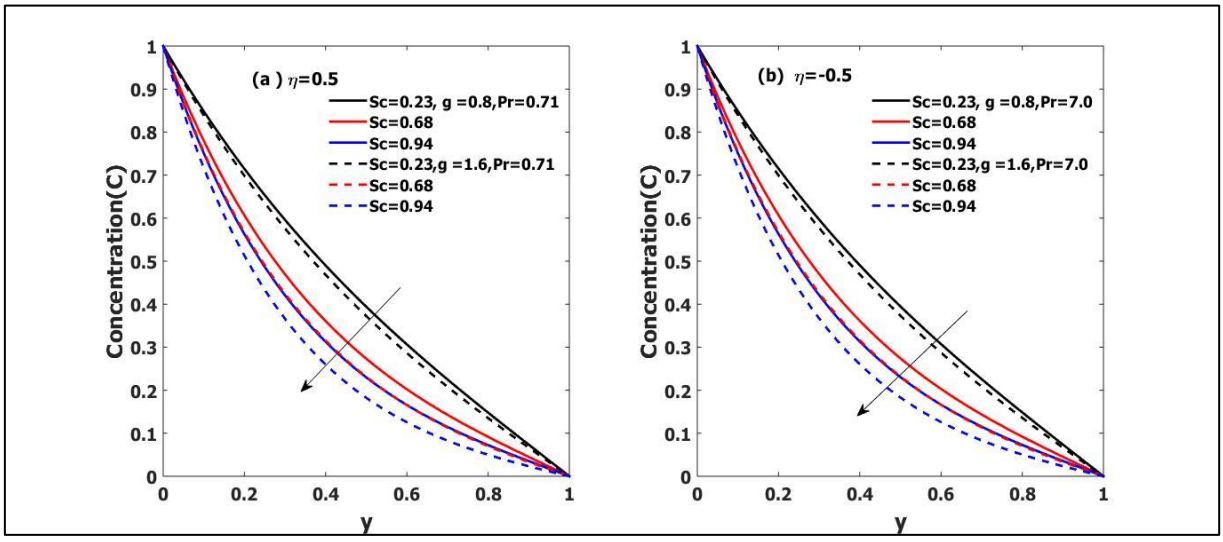

Figure 12: Interpretation of Schmidt number (Sc) on concentration profile

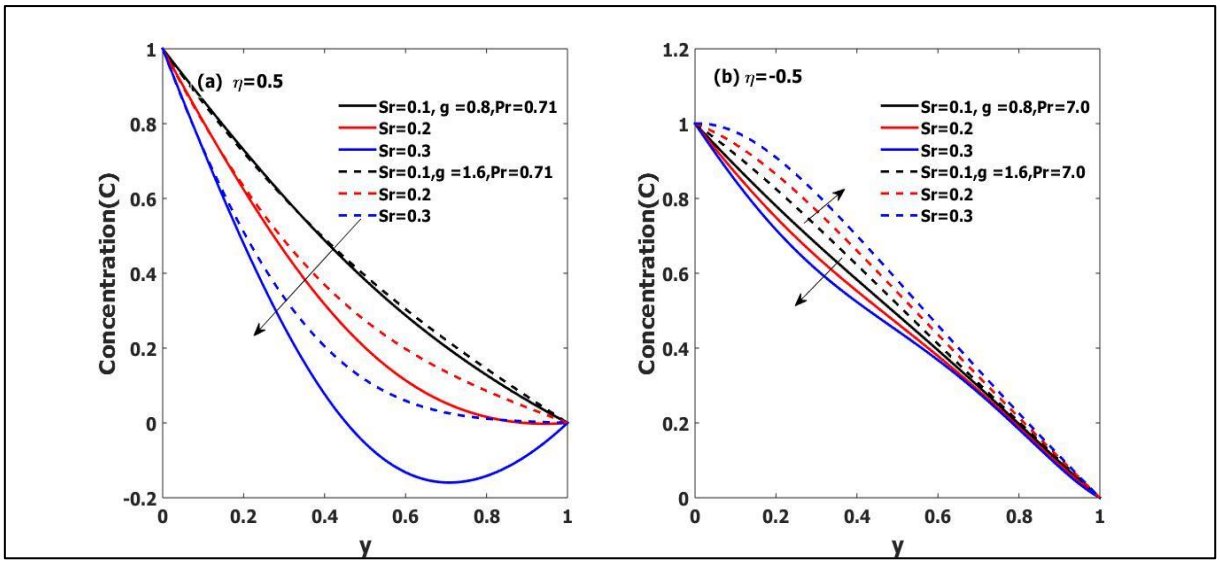

Figure 13: Interpretation of Soret number (Sr) on concentration profile

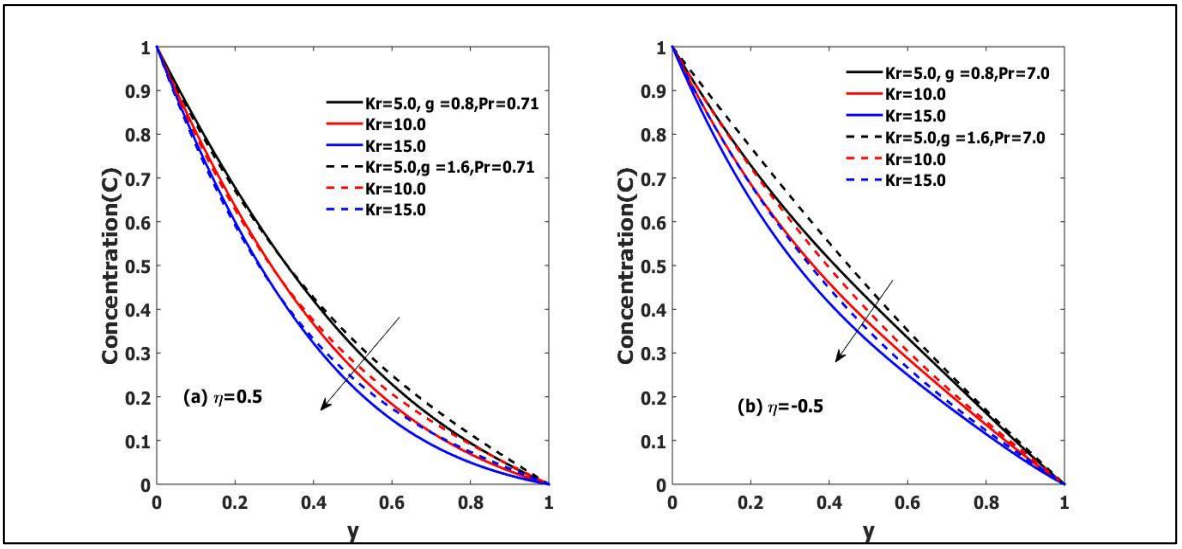

Figure 14: Interpretation of chemical reaction parameter (Kc) on concentration profile

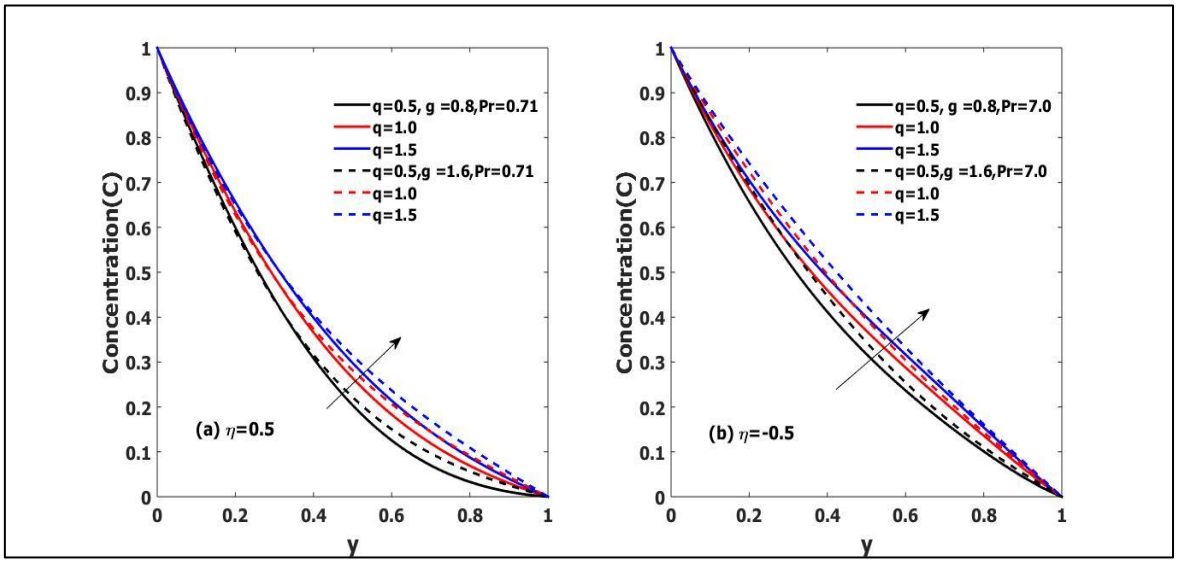

Figure 15: Interpretation of order of reaction parameter (q) on concentration profile

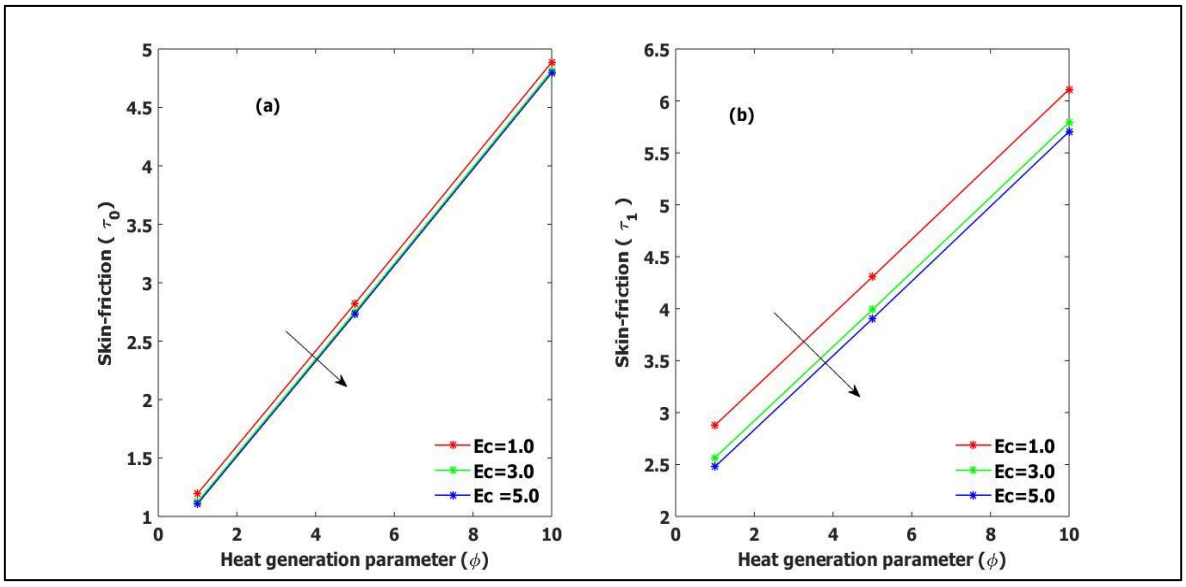

Figure 15: Interpretation of skin friction (τ) profile

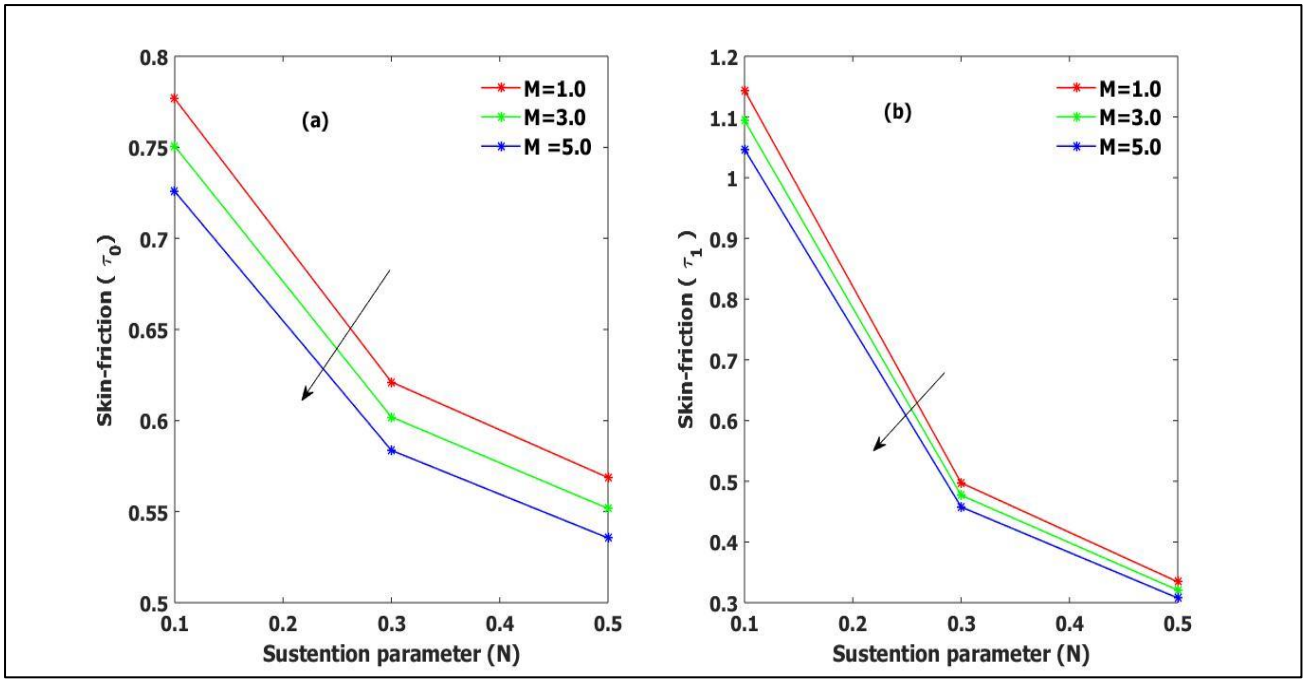

Figure 16: Interpretation of skin friction (τ) profile

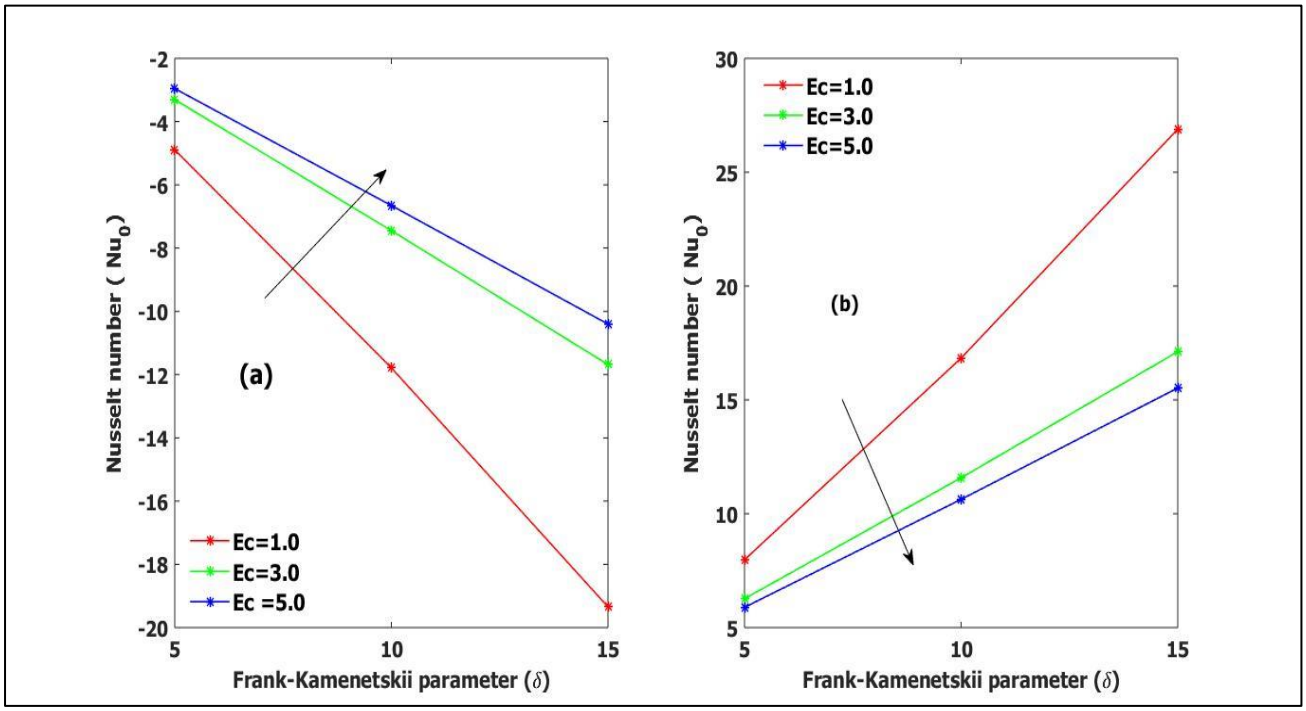

Figure 17: Interpretation of Nusselt number (N_u) profile

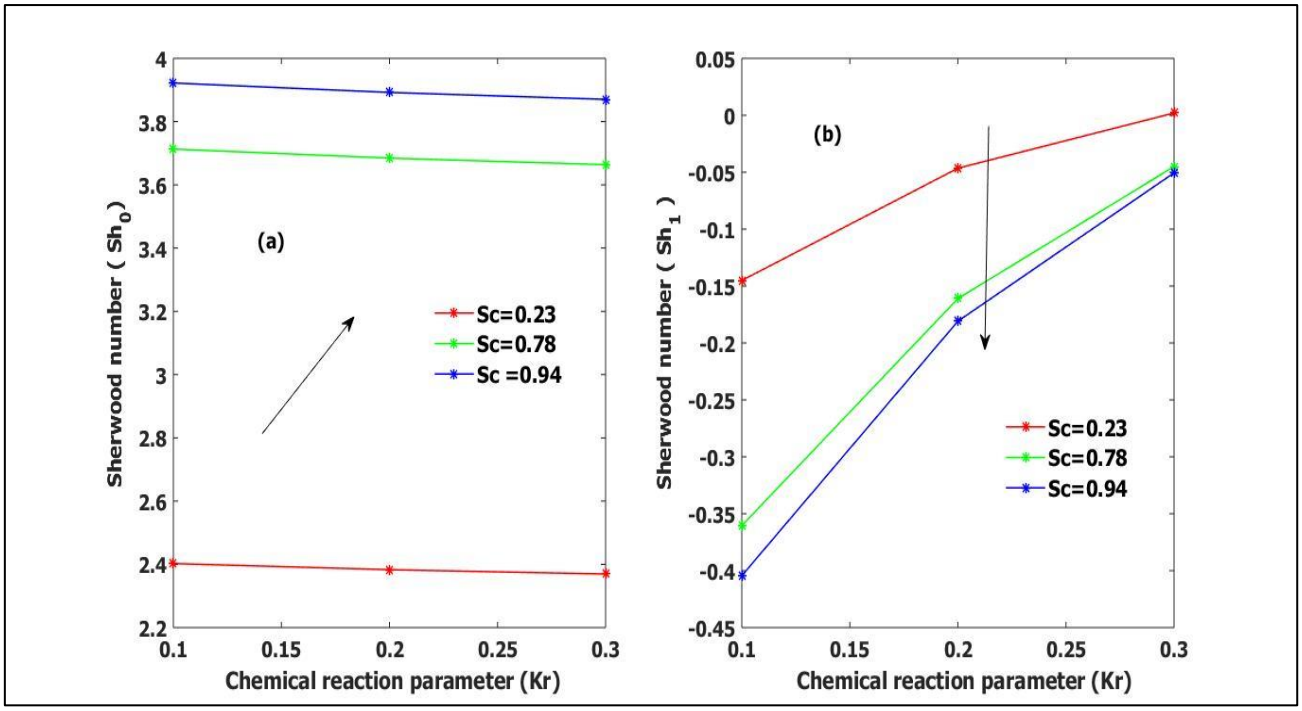

Figure 18: Interpretation of Sherwood number (S_h) profile

Figure 15 outlines the variation of skin friction (τ) at the plate $y=0$ and $y=1$.The plot indicates that, the skin friction (τ) decreases with the increasing Eckert number (Ec) and enhances with heat generation/sink parameter (ϕ) at the $y=0$ and $y=1$. The outcomes of the variation of the skin friction (τ) profile is demonstrated in Figure 16 at the $y=0$ and $y=1$. It is exhibited that the skin friction (τ) profile diminishes with magnetic parameter (M). Furthermore, from the plot the skin friction (τ) decreases with increasing sustention parameter (N) at the $y=0$ and $y=1$. The effect of Eckert number (Ec) on Nusselt number with reference to Frank-Kamenetskii parameter (δ) is graphed in Figure 17. It emphasized that, the increase in Eckert number (Ec) contributes to growths in Nusselt number at the plate $y=0$. It is further noticed that, as the Frank-Kamenetskii parameter (δ) increases the Nusselt number decreases. The reverse result is obtained at the plate $y=1$. The impression of Schmidt number (Sc) on Sherwood number is narrated in Figure 19(a) and 19(b). It is predicted that, the Schmidt number (Sc) alters as the Sherwood number increases. As well, increasing the chemical reaction parameter (Kc), the Sherwood number declines at plate $y=0$. The trend is reversed at the plate $y=1$.

5 CONCLUSIONS

In this manuscript, we have talked about the effect buoyancy ratio, magnetic field, suction and injection, heat generating/absorbing, variable viscosity parameter, variable thermal conductivity, Forchheimer parameter, power-law index and Frank-Kamenetskii parameter in a parallel vertical plate. Implicit finite difference is employed to obtain the numerical solution of the problem. Results obtained are validated and are found to be in good agreement with some existing problems. The summary of main findings of this investigation is:

- Velocity of the fluid growths for higher values of Da, λ and is diminishing with N and M.
- Temperature of the fluid enhances for varying values of γ, ϕ, δ, Du but falls with Pr and ε.
- The concentration of the fluid increases with q and decreases with Sc, Sr, and Kr.
- The skin friction is growing with ϕ and N and decreasing with M and Ec.
- The Nusselt number is increasing Ec and δ at y=0 and y=1 respectively.

REFERENCES

1. Khan, W. A., Culham, J. R., & Yovanovich, M. M. (2005). Fluid Flow Around and Heat Transfer from an Infinite Circular Cylinder. *ASME J. Heat Transfer*, 127, 785–790.
2. Acrivos, A., Shah, M. J., & Petersen, E. E. (1960). Momentum and Heat Transfer in Laminar Boundary-Layer Flows of Non-Newtonian Fluids Past External Surfaces. *AIChE J.*, 6, 312–317.
3. Schowalter, W. R. (1960). Application of Boundary-Layer Theory to Power- Law Pseudo-

Plastic Fluids: Similar Solutions. *AIChE J.*, 6, 24–28.
4. Shah, M. J., Petersen, E. E., & Acrivos, A. (1962). Heat Transfer from a Cylinder to a Power-Law Non-Newtonian Fluid. *AIChE J.*, 8, 542–549.
5. Acrivos, A., Shah, M. J., & Petersen, E. E. (1965). On Solution of Two- Dimensional Boundary-Layer Flow Equations for Non-Newtonian Power-Law Fluid. *Chem. Eng. Sci.*, 20, 101–105.
6. Lee, S. Y., & Ames, W. F. (1966). Similarity Solutions for Non-Newtonian Fluids. *AIChE J.*, 12, 700–708.
7. Abid, A., Memon, M., Asif, M., Kaleemullah, B., Tawfeeq Abdullah, A., Ilyas, K., & Afrasyab, K. (2021). Analysis of Power Law Fluids and the Heat Distribution on a Facing Surface of a Circular Cylinder Embedded in Rectangular Channel Fixed with Screen: A Finite Element's Analysis. *IEEE*, 9, DOI: 10.1109/ACCESS.2021.3076042
8. Nakayama, A. (1993). Free convection from a horizontal line heat source in a power-law fluid-saturated porous medium. *Int. J. of Heat and Fluid Flow*, 14, 279-283.
9. Sahu, A. K., & Mathur, M. N. (1996). Free convection in boundary layer flows of power law fluids past a vertical flat plate with suction/injection. *Indian Journal of Pure and Applied Mathematics*, 27, 931-941.
10. Rami, Y. J., & Arun, S. M. (2000). Free convection heat and mass transfer of non-Newtonian power law fluids with yield stress from a vertical flat plate in a saturated porous media. *Int. Commun. Heat Mass Transfer*, 27, 485-494.
11. Ching-Yang, C. (2006). Natural convection heat and mass transfer of non-Newtonian power-law fluids with yield stress in porous media from a vertical plate with variable wall heat and mass fluxes. *Int. Commun. Heat Mass Transfer*, 33, 1156-1164.
12. Kairi, R. R., & Murthy, P. V. S. N. (2009). Free Convection in a Thermally Stratified Non-Darcy Porous Medium Saturated with a Non-Newtonian Fluid. *Int. J. of Fluid Mech. Res*, 36(5).
13. Hyun, J. M., & Lee, J. W. (1990). Double-diffusive convection in a rectangle with cooperating horizontal gradients of temperature and concentration gradients. *Int. J. Heat Mass Transfer*, 33, 1605-1617.
14. Goyeau, A., Songbe, J. P., & Gobin, D. (1996). Numerical study of double-diffusive natural convection in a porous cavity using the Darcy Brinkman formulation. *Int. J. Heat Mass Transfer*, 39, 1363-1378.
15. Mamou, M., Vasseur, P., & Bilgen, E. (1996). Analytical and numerical study of double diffusive convection in a vertical enclosure. *Heat Mass Transfer*, 32, 115-125.
16. Ching-Yang, C. (2010). Double diffusive natural convection along an inclined wavy surface in a porous medium. *Int. Comm in Heat and Mass Transfer*, 37(10), 1471-1476.
17. Kays, W. M., & Grawford, M. E. (1980). Convection Heat and Mass Transfer, Pergamon, Oxford.
18. Chiam, T. C. (1996). Heat transfer with variable conductivity in a stagnation-point flow towards a stretching sheet, Int. Commun. *Heat Mass Transfer*, 23, 239–248.
19. Chiam, T. C. (1998). Heat transfer in a fluid with variable thermal conductivity over a linearly stretching sheet. *Acta Mech*, 129, 63–72.
20. Subhas, A., Prasad, K. V., & Mahaboob, A. (2005). Buoyancy force and thermal radiation effects in MHD boundary layer viscoelastic flow over continuously moving stretching surface. *Int. J. Therm. Sci.*, 44, 465–476.
21. Animasaun, I. L. (2015). Effects of thermophoresis, variable viscosity and thermal conductivity on free convective heat and mass transfer of non-Darci an MHD dissipative Casson fluid flow with suction and n^{th} order of chemical reaction. *Journal of the Nigerian Mathematical Society*, 34, 11–31.
22. Kiran Kumar, G., Srinivas, G., Babu, S., & Srikanth, G. (2018). Effects of Variable Viscosity and Thermal Conductivity on MHD Convective Heat Transfer of Immiscible Fluids in a Vertical Channel. *International Journal of Engineering Sciences & Research Technology*, 7(5), 73-73-79.
23. Ravi Chandra Babu, S. R., Venkateswarlu, S., & Jaya Lakshmi, K. (2018). Effect of Variable Viscosity and Thermal Conductivity on Heat and Mass Transfer Flow of Nano fluid over a Vertical Cone with Chemical Reaction. *International Journal of Applied Engineering Research*, 13(8), 13989-14002.
24. Choudhury, M., & Hazarika, G. C. (2013). The Effects of Variable Viscosity and Thermal Conductivity on MHD Oscillatory Free Convective Flow past a Vertical Plate in Slip Flow Regime with Variable Suction and Periodic Plate Temperature. *Journal of Applied Fluid Mechanics*, 6(2), 277-283.
25. Swain, K., Parida, S. K., & Dash, G. C. (2017). MHD Heat and Mass Transfer on Stretching Sheet with Variable Fluid Properties in Porous Medium. *AMSE JOURNALS-AMSE IIETA*, publication-2017-Series: Modelling B; 86(3), 706-726.